Osinga, H. M. (2001). Nonorientable manifolds in three-dimensional vector fields.

Nonorientable manifolds in three-dimensional vector fields

Hinke M Osinga
Department of Engineering Mathematics
University of Bristol
Bristol BS8 1TR, UK
H.M.Osinga@bristol.ac.uk

University of Bristol
ANM-Preinprint 2001.15

Revised version August 2002

Abstract

It is well-known that a nonorientable manifold in a three-dimensional vector field is topologically equivalent to a Möbius strip. The most frequently used example is the unstable manifold of a periodic orbit that just lost its stability in a period-doubling bifurcation. However, there are not many explicit studies in the literature in the context of dynamical systems, and so far only qualitative sketches could be given as illustrations. We give an overview of the possible bifurcations in three-dimensional vector fields that create nonorientable manifolds. We mainly focus on nonorientable manifolds of periodic orbits, because they are the key building blocks. This is illustrated with invariant manifolds of three-dimensional vector fields that arise from applications. These manifolds were computed with a new algorithm for computing two-dimensional manifolds.

Note that the quality of most of the figures in this preprint has been reduced substantially so that the electronic file has a reasonable size.

1 Introduction

In many applications one encounters models given as vector fields, that is, as systems of ODEs. Particularly when a system displays chaotic dynamics, one often needs to use numerical methods in order to understand its dynamics. Since it is virtually impossible to find an exact model, one is often interested in *qualitative* behavior and models are used to capture the *essential* dynamics in the simplest low-dimensional model. Classic examples are the Van der Pol equation, which models a simple electronic circuit exhibiting oscillations [Van der Pol, 1927], and the Lorenz system capturing the essence of complexity in weather models [Lorenz, 1963]. A more recent example is the study of a semiconductor laser with optical injection using the so-called rate equations; see [Wieczorek *et al.*, 1999] and further references therein. Very often, as is also the case with these examples, the resulting model is three-dimensional. The main reason for this is, probably, that three-dimensional vector fields are the lowest-dimensional continuous-time models that can exhibit extremely complicated behavior, including chaos.

To understand the dynamics of such a vector field, one typically looks for attractors, their basins of attraction and, in particular, the boundaries of these attracting domains. Two-dimensional invariant manifolds often act as basin boundaries, and it is important to know where they are located and what they look like. We call such manifolds *separating manifolds*, as they separate the state space into two invariant regions. Orbits starting on one side of the manifold are confined to this region since they cannot move through an invariant manifold.

It is important to note that not every two-dimensional invariant manifold is a separating manifold. In particular, a separating manifold must have two sides, namely an inside and an outside. However, there are two-dimensional manifolds that do not have two sides. Such manifolds are called *nonorientable* manifolds. The classical example of a nonorientable manifold is the Möbius strip, which is famous due to the illustration "Möbius Strip II" by M.C. Escher, reproduced in Fig. 1. Escher describes the Möbius strip as follows [Escher, 2000]:

> "An endless ring-shaped band usually has two distinct surfaces, one inside and one outside. Yet on this strip nine red ants crawl after each other and travel the front side as well as the reverse side. Therefore the strip has only one surface."

The Möbius strip is the only two-dimensional nonorientable manifold that can be embedded without self-intersections in $\mathbb{R}^3$. The mathematical definition of a nonorientable manifold is as follows. Consider an arbitrary closed path $\mathcal{C}(p_0)$ on a manifold M starting and ending at p_0, and choose a basis along $\mathcal{C}(p_0)$ of the tangent plane T_p at $p \in M$ that continuously depends on p. If the orientation of the basis, when it comes back to p_0 after moving along $\mathcal{C}(p_0)$, is the same as when we started, then M is called orientable. If for some point p_0 and some

This figure cannot be reproduced here due to copyright reasons.
Please see
http://www.escher.freeserve.co.uk/escher/MOEBIUS_BAND_II.jpg

Figure 1: *Probably the most famous nonorientable manifold is the Möbius strip with red ants, visualized by Escher in 1963.*

closed path $\mathcal{C}(p_0)$ the basis comes back with the reversed orientation, then M is called nonorientable; we refer to [Spivak, 1965] for more details.

A model of the Möbius strip, such as the one illustrated by M.C. Escher in Fig. 1, can easily be made by gluing the ends of a strip of paper together after giving it half a twist. Even though this strip, in practice, has finite width, it can theoretically be infinitely wide, that is, the Möbius strip does not necessarily have a boundary. Still, even an infinitely wide Möbius strip does not have an inside and an outside!

In this paper, we are interested in nonorientable manifolds in $\mathbb{R}^3$ that appear as stable or unstable manifolds of saddle points or saddle periodic orbits. The stable manifold of, say, a saddle periodic orbit Γ consists of points that converge to Γ under the flow of the associated vector field. Points on its unstable manifold have this property for the flow in backward time. A saddle equilibrium has a two-dimensional stable or unstable manifold, while the other manifold is one-dimensional. Stable and unstable manifolds of equilibria are always orientable. (Note that the closure of an orientable manifold may be nonorientable; see Sec. 6 for an example.) The stable and unstable manifolds of a saddle periodic orbit are both two-dimensional. They can be either orientable or nonorientable, depending on the Floquet multipliers of the saddle periodic orbit. The Floquet multiplier that corresponds to the phase shift along the periodic orbit is always 1. The other two Floquet multipliers are the eigenvalues of the corresponding fixed point of the Poincaré (first return) map; see also Fig. 2. If the periodic orbit is a saddle, both Floquet multipliers are real, one is inside the unit circle of the complex plane and the other is outside. The sign of the Floquet multiplier determines whether the associated manifold is orientable or not. Since the Poincaré map of a vector field in $\mathbb{R}^3$ is an orientation preserving map, the product of the Floquet multipliers must be positive. Hence, a saddle periodic orbit must either have two positive or two negative Floquet multipliers. This means that its two-dimensional (un)stable manifolds are either both orientable, and separating state space, or both nonorientable. We call a saddle periodic orbit with nonorientable (un)stable manifolds a *twisted* saddle periodic orbit.

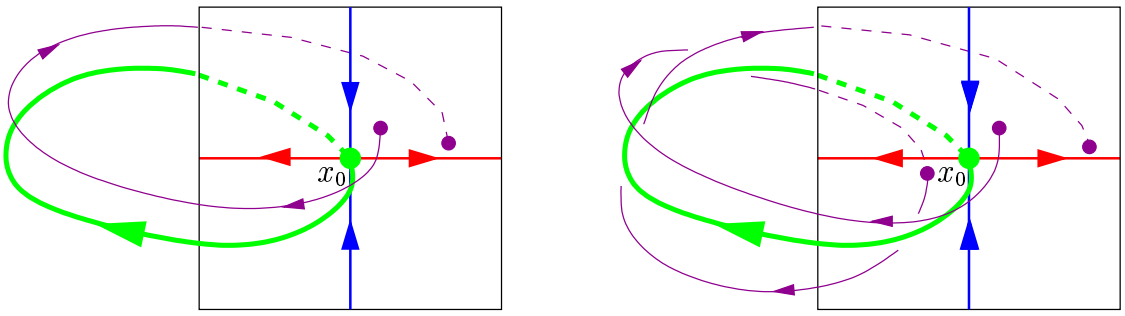

Positive Floquet multipliers:
the manifolds are orientable

Negative Floquet multipliers:
the manifolds are nonorientable

Figure 2: *Locally near a periodic orbit one can always define the Poincaré map or first return map on a section transverse to the periodic orbit. The image of a point on the section under this map is the next intersection point under the flow of the vector field. The periodic orbit is a fixed point x_0 of this map. If the periodic orbit is of saddle type, then the Jacobian of the map at x_0 has two real eigenvalues, one inside and one outside the unit circle. There are two cases, because the product of the eigenvalues must be positive. If the eigenvalues are positive, then points are mapped to the same side of the stable and unstable manifolds of x_0 (left); if they are negative, then the first intersection is on the diametrically opposite side of these manifolds (right).*

In this paper we are particularly interested in how nonorientable manifolds that are stable or unstable manifolds of a twisted saddle periodic orbit in a three-dimensional vector field appear or disappear as a parameter is varied. A well-known bifurcation that creates nonorientable manifolds is period-doubling. Here, an attracting periodic orbit loses its stability as one of its Floquet multipliers moves through -1. The periodic orbit becomes a twisted saddle periodic orbit and an attracting periodic orbit is created with twice the period. The nonorientable unstable manifold of the twisted saddle periodic orbit is bounded by this (non-twisted) period-doubled attractor. This scenario is described and illustrated in Sec. 3.

Another generic bifurcation that creates a twisted saddle periodic orbit with nonorientable stable and unstable manifolds is the twisted homoclinic bifurcation. This is a global bifurcation involving a homoclinic orbit. Details and illustrations of this bifurcation can be found in Sec. 4.

Once a twisted saddle periodic orbit with nonorientable manifolds exists, a saddle-node bifurcation may take place on the periodic orbit. This destroys the twisted saddle periodic orbit, but the nonorientable manifolds persist; more details are given in Sec. 6.

The nonorientable manifolds shown in this paper are numerical approxima-

tions of actual invariant manifolds of a vector field. The algorithm that is used for these computations was developed only recently; see [Krauskopf & Osinga, 1999] and [Osinga, 2000]. We contrast illustrations of manifolds in the full three-dimensional state space with pictures of one-dimensional equivalents of the nonorientable manifolds in suitable Poincaré sections. The one-dimensional manifolds are computed with the algorithm described in [Krauskopf & Osinga, 1998], which is implemented for use in the DsTool environment [Krauskopf & Osinga, 2000].

This paper is organized as follows. In the next section we give the notation and background for the study of nonorientable manifolds. The bifurcations of periodic orbits that *create* nonorientable manifolds are illustrated with examples in sections 3 and 4; see also the multimedia supplement [Osinga, 2002] for animations of the manifolds. Section 5 contrasts three-dimensional vector fields with two-dimensional diffeomorphisms and gives examples of orientable manifolds as well. In Sec. 6 we consider nonorientable invariant manifolds that are not stable or unstable manifolds of a periodic orbit. Finally, in Sec. 7 we briefly discuss the situation for higher-dimensional vector fields. The numerical method for computing nonorientable stable or unstable manifolds of a twisted saddle periodic orbit is summarized in the Appendix.

Throughout this paper a color-coding is used to enhance the understanding of the illustrations: all saddle periodic orbits are shown in green and their stable and unstable manifols are blue and red, respectively.

2 Notation and Background

We study nonorientable invariant manifolds of a twisted saddle periodic orbit in a three-dimensional vector field of the form

$$\dot{x} = f(x, \alpha). \tag{1}$$

Here, $x \in \mathbb{R}^3$, $\alpha \in \mathbb{R}$ is a parameter, and $f : \mathbb{R}^3 \times \mathbb{R} \mapsto \mathbb{R}^3$ is sufficiently smooth.

Note that any nonorientable manifold M in $\mathbb{R}^3$ must be two-dimensional. Furthermore, since M lives in $\mathbb{R}^3$, M is topologically equivalent to a Möbius strip; a Klein bottle can only be embedded in a space of dimension at least four. A topological Möbius strip that is invariant under the flow of (1) (for some fixed α) can either be bounded or infinitely long; both cases are illustrated in Sec. 3.

We assume that (1) has a twisted saddle periodic orbit Γ for some $\alpha = \alpha_0$. This means that Γ has one real negative Floquet multiplier $\lambda^u < -1$ and one real negative Floquet multiplier $-1 < \lambda^s < 0$. This is because, as was mentioned in the introduction, the product of the Floquet multipliers of any periodic orbit must be positive. Hence, the stable and unstable manifolds of Γ are both two-dimensional and nonorientable, that is, topologically equivalent to a Möbius strip.

Twisted saddle periodic orbits are structurally stable. In other words, there exists an (open) interval I_α around α_0 for which Γ_α is a twisted saddle periodic

orbit with nonorientable stable and unstable manifolds. Namely, the implicit function theorem and the hyperbolicity of Γ guarantee the existence of Γ_α, while also the Floquet multipliers vary continuously with α.

We are interested in how nonorientable manifolds are created or destroyed in such a parameter-dependent setting. It may seem restrictive to limit our study to stable or unstable manifolds of twisted periodic orbits Γ_α, but the manifolds of Γ_α turn out to be the key building blocks for nonorientable manifolds of vector fields in $\mathbb{R}^3$; see also Sec. 6. Hence, we ask what happens to Γ_α at the endpoints of I_α, where the twisted saddle periodic orbit is created or destroyed. There are only three possible bifurcations:

1. Period-doubling bifurcation.
   One Floquet multiplier moves through -1. The nonorientable unstable (stable) manifold of the twisted saddle periodic orbit Γ_α disappears as Γ_α becomes stable (unstable). The periodic orbit together with its nonorientable strong stable (unstable) manifold persists. The period-doubling bifurcation is illustrated in Sec. 3.

2. Twisted homoclinic bifurcation.
   In a *twisted* homoclinic bifurcation a *twisted* periodic orbit hits an equilibrium, its period becomes infinite, and the periodic orbit disappears. With the periodic orbit both nonorientable stable and unstable manifolds disappear. The bifurcation is illustrated in Sec. 4.

3. Saddle-node bifurcation on a limit cycle.
   Two equilibria appear on the twisted saddle periodic orbit, which are both saddles, one with two stable eigenvalues and the other with two unstable eigenvalues. Even though the periodic orbit disappears, the nonorientable manifolds persist as the closure of the two-dimensional orientable stable and unstable manifolds of the two saddle points. More details can be found in Sec. 6.

Since nonorientable manifolds are associated with negative Floquet multipliers, one could assume that these multipliers change sign at the endpoints of I_α. However, a Floquet multiplier cannot simply move through 0, because this would make the vector field degenerate. (Even worse, both multipliers would be required to change sign simultaneously.) The only way for the Floquet multipliers to change sign is to move as a complex conjugated pair through the imaginary axis. This cannot happen for a saddle periodic orbit, so that first a different bifurcation must take place. Note that, at the moment when a pair of complex conjugated Floquet multipliers collides on the negative real axis, such that both multipliers become real and negative, a strong (un)stable manifold is created that is nonorientable. This scenario is, in fact, a typical prelude to the (supercritical) period-doubling bifurcation, when an attracting periodic orbit becomes unstable creating a period-doubled attracting periodic orbit; see also Sec. 3.

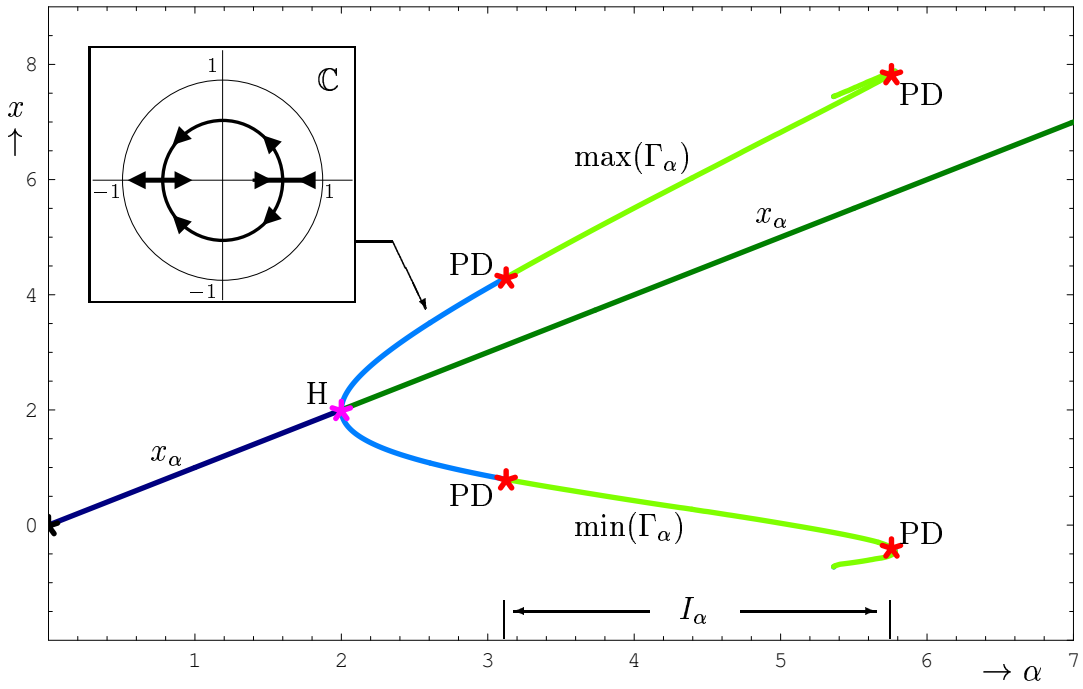

Figure 3: *The (partial) bifurcation diagram for the ζ^3-model (2). The periodic orbit Γ_α emanating from the branch x_α is attracting for $2 < \alpha < 3.125$ (blue). Both the maximal and minimal x-coordinates are shown. The inset illustrates how the (stable) Floquet multipliers change between the Hopf bifurcation (H) and the first period-doubling bifurcation (PD). The periodic orbit Γ_α is a twisted saddle (green) for $\alpha \in I_\alpha \approx (3.125, 5.757)$. The attracting period-doubled orbit Ω_α is not shown.*

There are other bifurcations that create periodic orbits [Kuznetsov, 1995]: the saddle-node bifurcation of limit cycles, the Hopf bifurcation, and the Neimark-Sacker or torus bifurcation. However, none of the periodic orbits involved are twisted saddle periodic orbits.

3 Period-Doubling Bifurcation

We now illustrate the creation of nonorientable manifolds via a scenario involving a period-doubling bifurcation in the model

$$\begin{cases} \dot{x} &= y, \\ \dot{y} &= z, \\ \dot{z} &= \alpha\, x - x^2 - \beta\, y - z. \end{cases} \tag{2}$$

This vector field is the asymptotic normal form of a system near the simultaneous onset of up to three instabilities, known as the ζ^3-model [Arneodo *et al.*, 1985].

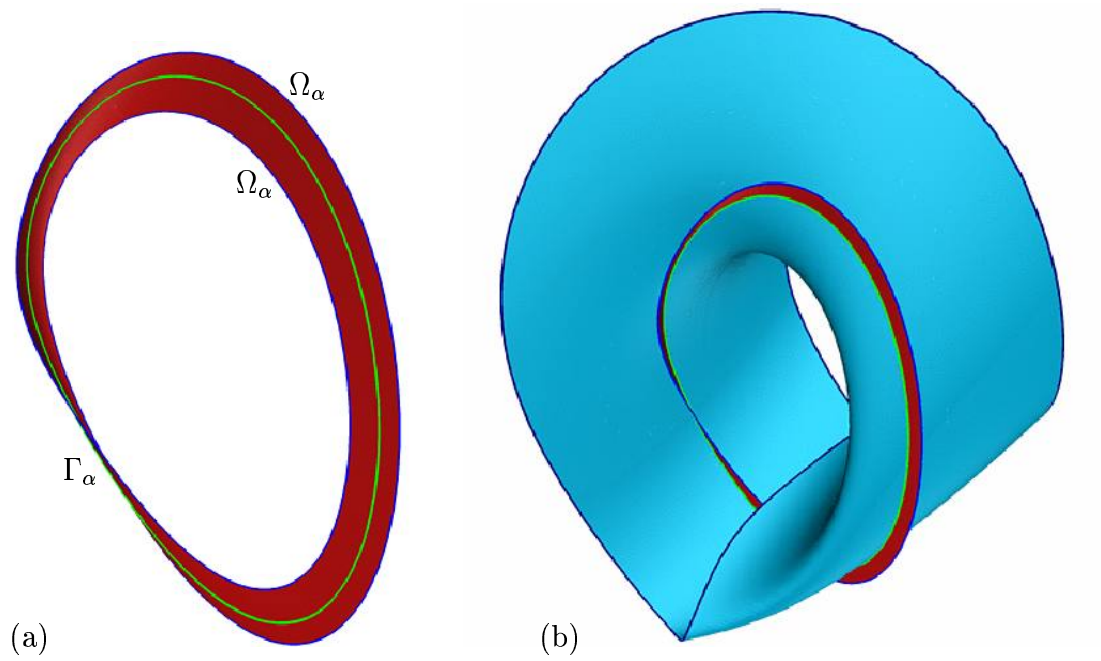

Figure 4: *The nonorientable unstable manifold (red) of the periodic orbit* Γ_α *(green) in the* ζ^3*-model (2) for* $\alpha = 3.2$ *(a). This manifold is bounded by the period-doubled attractor* Ω_α *(blue). (b) The unstable manifold together with the stable manifold of* Γ_α*. The stable manifold (blue) is unbounded; the boundary of the piece that was computed is highlighted for clarity only.*

This system was used as an example in [Glendinning & Sparrow, 1984] for a detailed study of Shil′nikov homoclinic orbits. Two-dimensional orientable manifolds were computed for $\beta = 2$ and various choices of α in [Johnson *et al.*, 1997] and [Krauskopf & Osinga, 1999]. As in the former two papers, we fix $\beta = 2$ and let α be the continuation parameter.

Figure 3 gives a partial bifurcation diagram for Eq. (2) with $\beta = 2$. There are two equilibria, the origin (not shown in Fig. 3) and $x_\alpha = (\alpha, 0, 0)$. A transcritical bifurcation (black star) takes place at $\alpha = 0$ such that, for $\alpha > 0$, the origin is a saddle and x_α is attracting (dark blue) until it undergoes a (supercritical) Hopf bifurcation at $\alpha = \beta$, indicated by the pink star. The Hopf bifurcation creates an attracting periodic orbit Γ_α (blue) that becomes a twisted saddle (green) in a period-doubling bifurcation at $\alpha \approx 3.125$ (red stars). Note that a period-doubled attracting periodic orbit appears which is not shown in Fig. 3, but which we shall refer to as Ω_α. The period-doubled orbit Ω_α rapidly undergoes further period-doubling bifurcations to chaos and only exists as an attractor for $\alpha \in (3.125, 3.357)$. The interval I_α for which Γ_α is a twisted saddle periodic orbit ends at a second period-doubling bifurcation, at $\alpha \approx 5.757$, where Γ_α becomes attracting again. In this region complicated Shil′nikov behaviour exists involving

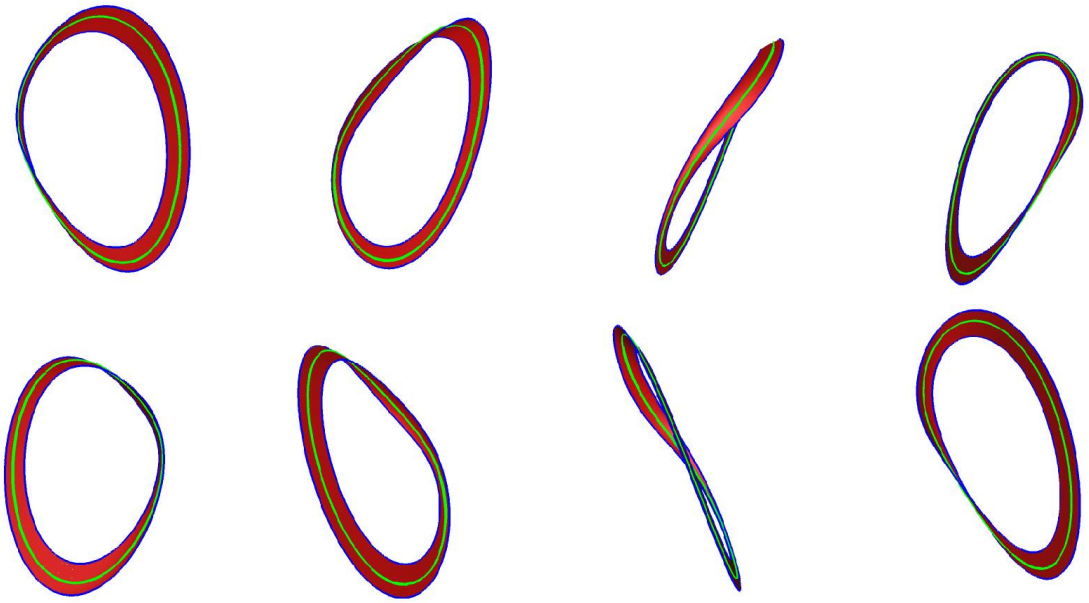

Figure 5: *Rotations about the z-axis centered at x_α of the nonorientable unstable manifold (red) of the twisted saddle periodic orbit Γ_α (green) in the ζ^3-model (2) for $\alpha = 3.2$. This manifold is bounded by a period-doubled periodic orbit (blue). The viewpoints are the same as those in Fig. 6 with the bottom-right picture as in Fig. 4(a).*

homoclinic orbits to the origin, which is accompanied by other period-doubling bifurcations; we refer to [Glendinning & Sparrow, 1984] for more details on the bifurcation structure.

To illustrate the nonorientable manifolds after the first period-doubling bifurcation, we computed both stable and unstable manifolds of Γ_α for $\alpha = 3.2$; see Fig. 4. The Floquet multipliers are $\lambda^s_\alpha \approx -0.008$ and $\lambda^u_\alpha \approx -1.158$ in this case. The unstable manifold is shown in red. It is bounded by the period-doubled attracting periodic orbit Ω_α (blue). The stable manifold of Γ_α is shown in blue and it is unbounded. Figure 4(b) shows the part of the stable manifold that was computed. Animations of the manifolds can be found in the multimedia supplement [Osinga, 2002]. Snapshots of these animations are shown in Figs. 5 - 7. Figure 5 shows the unstable manifold of Γ_α rotating about the z-axis, centered at x_α. The corresponding snapshots of this same rotation for both $W^s(\Gamma_\alpha)$ and $W^u(\Gamma_\alpha)$ is shown in Fig. 6.

Note that the period-doubling bifurcation as a mechanism for creating nonorientable manifolds does not create a twisted periodic orbit. The period-doubled orbit that is created in this bifurcation is always non-twisted. The twisted periodic orbit already exists in a neighborhood of the bifurcation, and only changes from attracting (in this example) to saddle-type. It is created in a Hopf bifur-

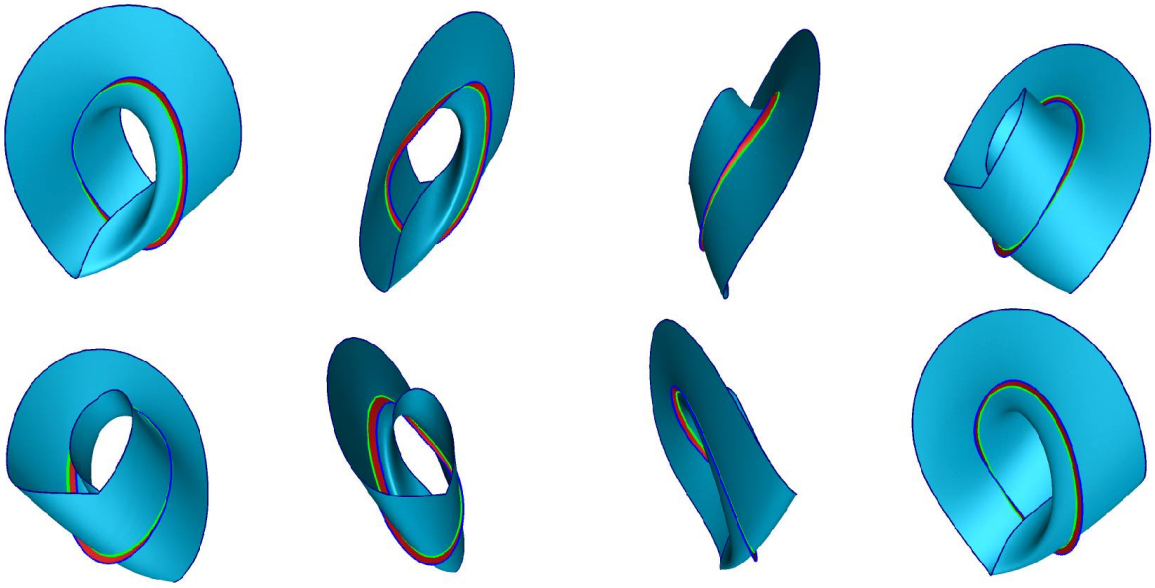

Figure 6: *Rotations about the z-axis centered at x_α of both the nonorientable stable (blue) and unstable (red) manifolds of the twisted saddle periodic orbit Γ_α (green) in the ζ^3-model (2) for $\alpha = 3.2$. The unstable manifold is bounded but the stable manifold is not; the boundary of the piece that was computed is highlighted for clarity only. The viewpoints are the same as those in Fig. 5 with the bottom-right picture as in Fig. 4(b).*

cation and, initially has two real and positive stable Floquet multipliers. The smallest one is associated with the strong stable manifold of the periodic orbit, which is a two-dimensional orientable manifold. As α increases, the two stable Floquet multipliers coalesce on the positive real axis and become complex conjugated, after which the strong stable manifold ceases to exist. Subsequently, this pair of complex conjugated Floquet multipliers moves through the imaginary axis. This means that trajectories on the three-dimensional stable manifold spiral around as they accumulate on the attracting periodic orbit. Successive intersections of these orbits with a Poincaré section converge to the periodic orbit with a rate determined by the modulus of the Floquet multipliers, and rotate with a relative angle dictated by the argument, that is, the ratio of the real and imaginary part. As the Floquet multipliers move through the imaginary axis, this angle becomes larger. It is exactly π radians when the stable Floquet multipliers coalesce again on the negative real axis. For larger α, the Floquet multipliers are real and negative; a two-dimensional strong stable manifold again exists and is now nonorientable. The behavior of the two Floquet multipliers as α increases is illustrated in the inset of Fig. 3.

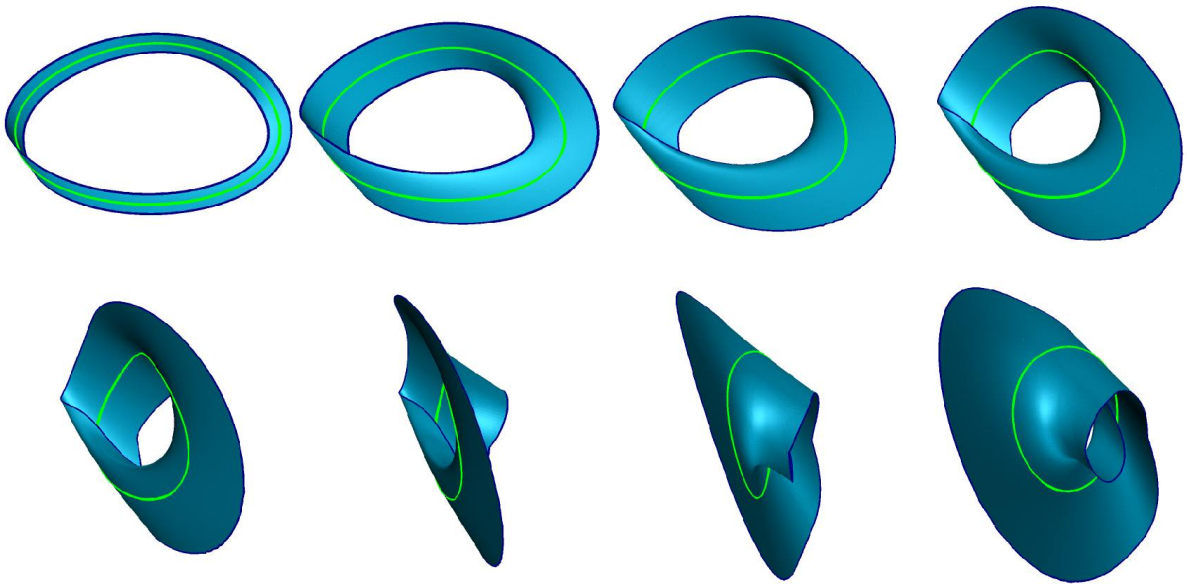

Figure 7: *Several stages of the computation of the unbouned nonorientable stable manifold (blue) of the twisted saddle periodic orbit* Γ_α *(green) in the* ζ^3*-model (2) for* $\alpha = 3.2$*. The stable manifold grows and we zoom out as the manifold is rotated about the z-axis centered at* x_α*. In each picture the boundary of the piece that is computed so far is highlighted for clarity.*

We can already speak of a twisted periodic orbit when both stable Floquet multipliers are real and negative. Hence, in between the Hopf bifurcation and the period-doubling bifurcation, at the moment when the two stable Floquet multipliers coalesce on the negative real axis, a twisted periodic orbit is created. At this moment, a nonorientable manifold appears, namely the strong stable manifold of the attracting periodic orbit. The period-doubling bifurcation marks the transition of Γ_α from a twisted attractor to a twisted saddle periodic orbit. The stable manifold of Γ_α can be considered as a continuation of the strong stable manifold. The nonorientable unstable manifold of Γ_α is created in the period-doubling bifurcation.

4 Twisted Homoclinic Bifurcation

In a homoclinic bifurcation a periodic orbit disappears as it hits a saddle equilibrium. At the moment of the bifurcation the periodic orbit has infinite period and is, in fact, a homoclinic orbit to the saddle point. In three-dimensional vector fields this homoclinic orbit is formed by the one-dimensional unstable manifold that comes back along the two-dimensional stable manifold. (If the saddle has

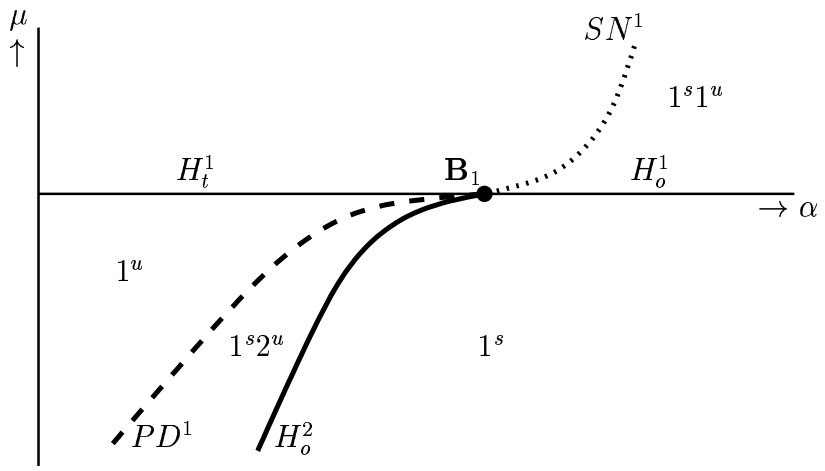

Figure 8: *Sketch of the unfolding of the codimension-two inclination flip bifurcation point* $\mathbf{B}_1 \approx (1.193, 0)$ *for Sandstede's model (3) in the* (α, μ)*-plane; notation is as in [Oldeman* et al.*, 2000].*

two unstable eigenvalues, then this holds for the time-reversed system.) In contrast to homoclinic orbits in two-dimensional vector fields, there are now two geometrically different possibilities: the two-dimensional stable manifold, when followed along the homoclinic orbit is either orientable, that is topologically a cylinder, or nonorientable such that it forms a Möbius strip. Consequently, we speak of *oriented* (the former) and *twisted* (the latter) homoclinic bifurcations. The periodic orbit that exists before the homoclinic bifurcation is a saddle. For the twisted homoclinic bifurcation it is twisted, while for the oriented homoclinic bifurcation it is not.

The twisted homoclinic bifurcation is illustrated with an example that is known as Sandstede's model [Sandstede, 1997]. This model is used to study orbit flip and inclination flip bifurcations, which are both of codimension two. In the unfolding of either one of these codimension-two bifurcation points a curve of homoclinic bifurcations exist that changes from oriented to twisted. We choose to work with the unfolding of an inclination flip bifurcation and use parameters as in table 2 of [Oldeman *et al.*, 2000]. In this case, Sandstede's model can be written as

$$\left\{ \begin{array}{rcl} \dot{x} &=& ax + by - ax^2 - \alpha xz(2 - 3x), \\ \dot{y} &=& bx + ay - \frac{3}{2}bx^2 - \frac{3}{2}axy + 2\alpha yz, \\ \dot{z} &=& cz + \mu x + \gamma xz + \alpha\beta(x^2(1 - x) - y^2). \end{array} \right. \tag{3}$$

Here $a = 0.125$, $b = 0.875$, $c = -2$, $\beta = 1$ and $\gamma = 3$ as in [Oldeman *et al.*, 2000]. For these parameters the origin is always a saddle equilibrium with a two-dimensional manifold denoted by $W^s(0)$. Figure 8 shows a sketch of the codimension-two unfolding in the (α, μ)-plane in a small neighborhood of the codimension-

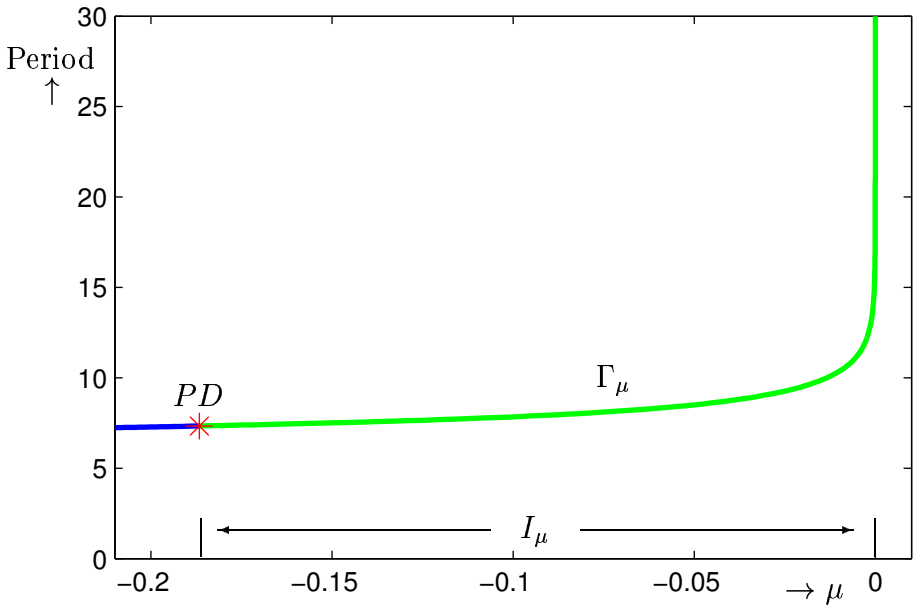

Figure 9: *The bifurcation diagram for Sandstede's model (3) with* $\alpha = 1$ *showing the period of* Γ_μ *versus* μ. *The twisted saddle periodic orbit* Γ_μ *(green) becomes stable in a period-doubling bifurcation (red star); the period-doubled orbit is not shown. As the period goes to infinity,* Γ_μ *disappears in a twisted homoclinic bifurcation at* $\mu = 0$.

two bifurcation point $\mathbf{B}_1$ which lies on the μ-axis at $\alpha \approx 1.193$; compare also Fig. 9 of [Oldeman *et al.*, 2000]. We use the notation of [Oldeman *et al.*, 2000] to indicate the (relative) period of the periodic orbits that exist in the various regions. The superscripts s and u stand for stable and unstable (of saddle type, in fact) and the subscripts o and t mean orientable and twisted, respectively.

Our interest is in a crossing of the H_t^1 curve. A (primary) twisted saddle periodic orbit Γ_μ with nonorientable stable and unstable manifolds exists in between the curves PD^1 and H_t^1. Figure 9 shows a bifurcation diagram for $\alpha = 1$ where the period of the periodic orbit is plotted versus μ. The periodic orbit Γ_μ is a twisted saddle periodic orbit for $\mu \in I_\mu \approx (-0.187, 0)$. At the twisted homoclinic bifurcation Γ_μ hits the origin and its period has become infinite. This destroys Γ_μ. Note that, in contrast to the period-doubling bifurcation, where one of the two nonorientable manifolds exists on either side of the bifurcation, the twisted homoclinic bifurcation not only causes the disappearance of Γ_μ, but both its nonorientable stable and unstable manifolds disappear as well.

Just before the twisted homoclinic bifurcation there are two stable manifolds in the system, namely the (orientable) stable manifold $W^s(0)$ of the origin and the nonorientable stable manifold $W^s(\Gamma_\mu)$ of Γ_μ. Figure 10 shows these two manifolds for $\alpha = 1$ and $\mu = -0.01$. We should think of $W^s(0)$ as consisting of

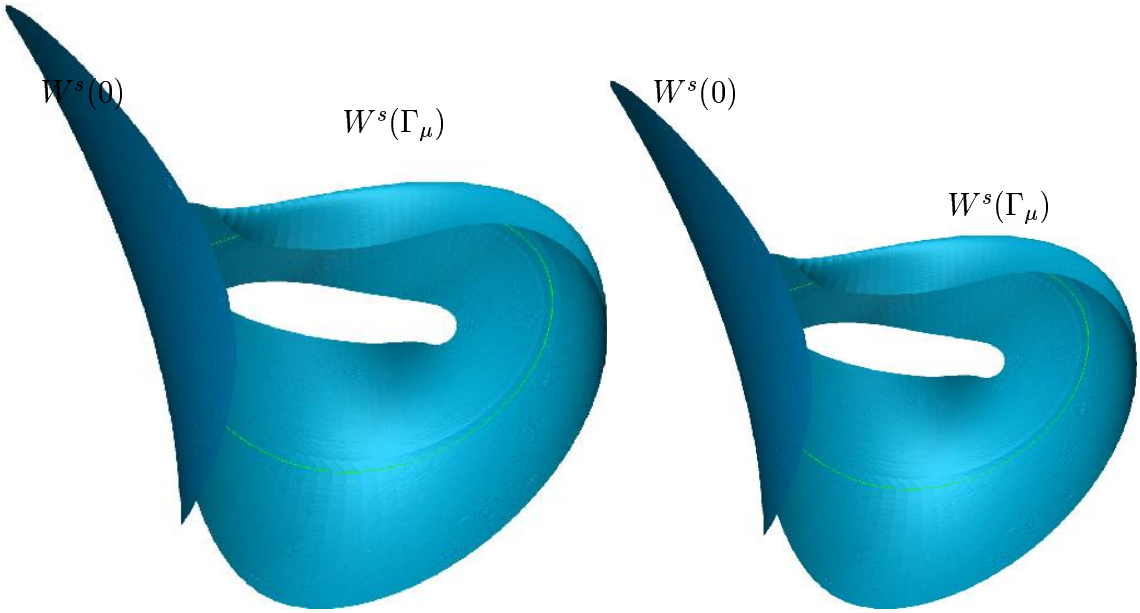

Figure 10: *Two different viewpoints of the stable manifolds in Sandstede's model (3) for* $\alpha = 1$ *and* $\mu = -0.01$ *near a twisted homoclinic bifurcation at* $\mu = 0$, *where* Γ_μ *(green) hits the origin. The stable manifold* $W^s(0)$ *of the origin is orientable and the stable manifold* $W^s(\Gamma_\mu)$ *of* Γ_μ *is nonorientable.*

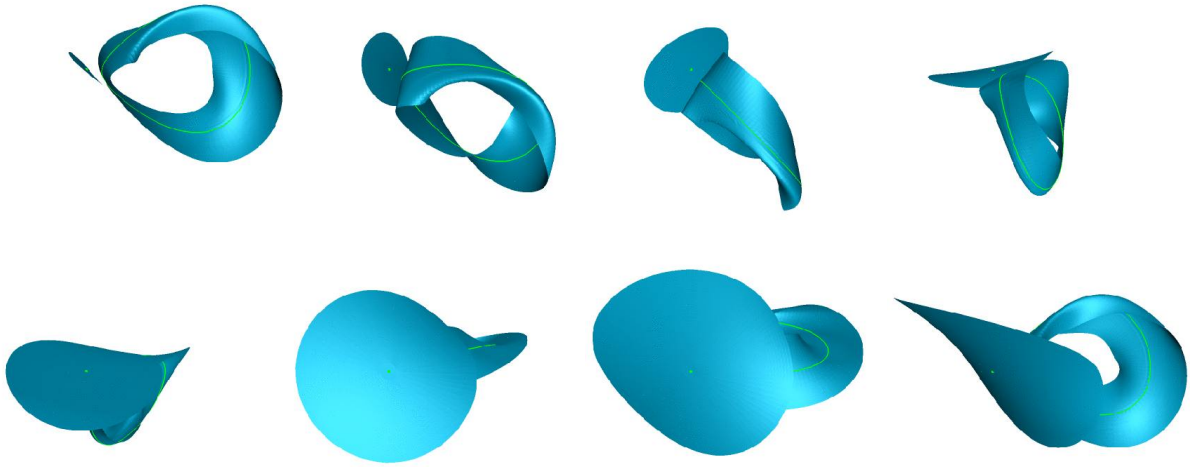

Figure 11: *The nonorientable stable manifold of the twisted saddle periodic orbit* Γ_μ *(green) in Sandstede's model (3) for* $\alpha = 1$ *and* $\mu = -0.01$ *is very close to the orientable stable manifold of the origin. Snapshots give an impression of one full rotation about the line perpendicular to the plane* $x = y + 2z$, *while* $W^s(0)$ *grows and accumulates on* $W^s(\Gamma_\mu)$.

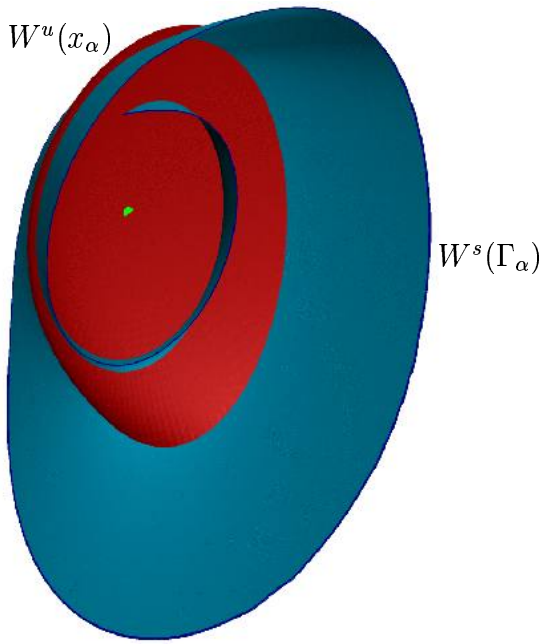

Figure 12: *The ζ^3-model (2) for $\alpha = 3.2$ showing the nonorientable stable manifold $W^s(\Gamma_\alpha)$ (blue) together with the two-dimensional unstable manifold (red) of the equilibrium x_α (green). Note that Γ_α is hidden by $W^u(x_\alpha)$.*

two halves, separated by the one-dimensional strong stable manifold. One half goes off to infinity. The other half accumulates on $W^s(\Gamma_\mu)$ by winding around Γ_μ, making half a twist at each turn. The animation in the associated multimedia supplement [Osinga, 2002] grows $W^s(0)$ while it closely follows $W^s(\Gamma_\mu)$. Snapshots of this animation are shown in Fig. 11.

After the twisted homoclinic bifurcation, $W^s(\Gamma_\mu)$ no longer exists. At $\mu = 0$ the nonorientable stable manifold of Γ_μ becomes half of $W^s(0)$. In other words, $W^s(0)$ folds back onto itself with half a twist.

5 Vector Fields versus Diffeomorphisms

It is common in the literature to study periodic orbits in a three-dimensional vector field via the corresponding fixed points of a two-dimensional map. Indeed, the two-dimensional map is obtained as the Poincaré or first return map on a suitably defined section transverse to the periodic orbit. Even though the study of generic two-dimensional diffeomorphisms has created good intuition of what can happen in planar discrete systems, it cannot always be translated to corresponding behavior in three-dimensional vector fields.

To illustrate this, we consider the two-dimensional (orientable) unstable manifold of the equilibrium $x_\alpha = (\alpha, 0, 0)$ in the ζ^3-model (2) for $\alpha = 3.2$. This mani-

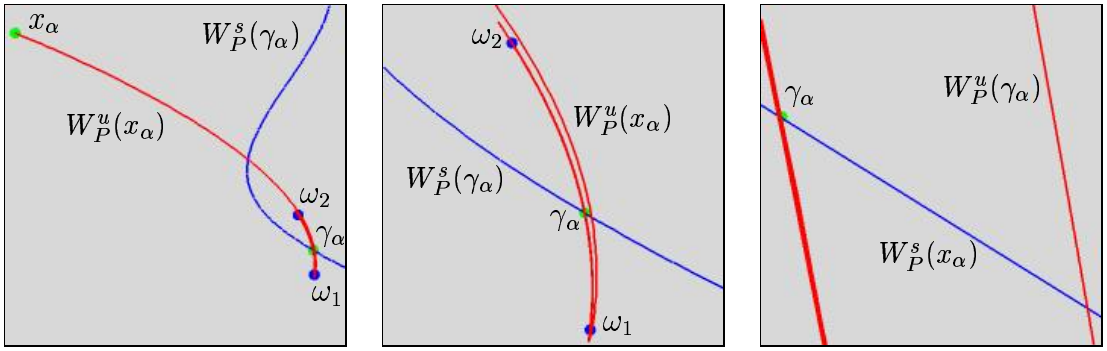

Figure 13: *The stable manifold (blue) of γ_α and the unstable manifold (red) of x_α in the Poincaré section $\mathcal{S}_P = \{y = 0\}$ for $\alpha = 3.2$ (a). Enlargements in (b) and (c) show that $W^u_P(x_\alpha)$ winds around the period-two attractor $\{\omega_1, \omega_2\}$ from the outside going in so that is intersects $W^s_P(\gamma_\alpha)$ on both sides of γ_α.*

fold accumulates on the period-doubled limit cycle Ω_α. In fact, it accumulates on the closure of $W^u(\Gamma_\alpha)$, that is, on the Möbius strip made up by Γ_α, $W^u(\Gamma_\alpha)$, and Ω_α. As a consequence, there is a generic heteroclinic intersection between this manifold and the nonorientable stable manifold $W^s(\Gamma_\alpha)$ of Γ_α; see Fig. 12. Since two unstable manifolds cannot intersect, $W^u(x_\alpha)$ must wind around $W^u(\Gamma_\alpha)$, and even around the closure of $W^u(\Gamma_\alpha)$. Hence, Γ_α, $W^u(\Gamma_\alpha)$ and Ω_α are covered by $W^u(x_\alpha)$ and cannot be seen in Fig. 12.

In order to see the geometry of these manifolds, we should look at a cross-section transverse to $W^u(x_\alpha)$, so that we can see the other manifolds inside. To this end, we define a Poincaré section $\mathcal{S}_P$ that is transverse both to $W^u(x_\alpha)$ and Γ_α. In fact, $\mathcal{S}_P$ should be such that is contains x_α. We now define the Poincaré or first return map P on $\mathcal{S}_P$, where we take $P(x_\alpha) = x_\alpha$. This means that both x_α and $\gamma_\alpha := \Gamma_\alpha \cap \mathcal{S}_P$ are fixed points of P. The period-doubled attractor Ω_α corresponds to a period-two point of P. Furthermore, x_α and γ_α have one-dimensional stable and unstable manifolds. These manifolds are the intersections of the corresponding two-dimensional manifolds in the full state space with $\mathcal{S}_P$. We define $W^s_P(\gamma_\alpha) = W^s(\Gamma_\alpha) \cap \mathcal{S}_P$ and $W^u_P(x_\alpha) = W^u(x_\alpha) \cap \mathcal{S}_P$.

Figure 13 shows the intersection of Fig. 12 with the Poincaré section $\mathcal{S}_P$ defined as $\{y = 0\}$. The two intersection points of Ω_α with $\mathcal{S}_P$ for $\alpha = 3.2$ are denoted by ω_1 and ω_2. The unstable manifold of x_α oscillates back and forth between these two points, so that it accumulates on the unstable manifold of γ_α. Therefore, $W^u(x_\alpha)$ must intersect $W^s_P(\gamma_\alpha)$. Figure 14 gives an idea of how the one-dimensional manifolds $W^u_P(x_\alpha)$ vary continuously with the Poincaré sections $\mathcal{S}_P(\varphi)$ along Γ_α, where φ is the angle with the z-axis. Here, only x_α, $W^u_P(x_\alpha)$, and the period-doubled attractor $\{\omega_1, \omega_2\}$ are shown. Figure 13 corresponds with

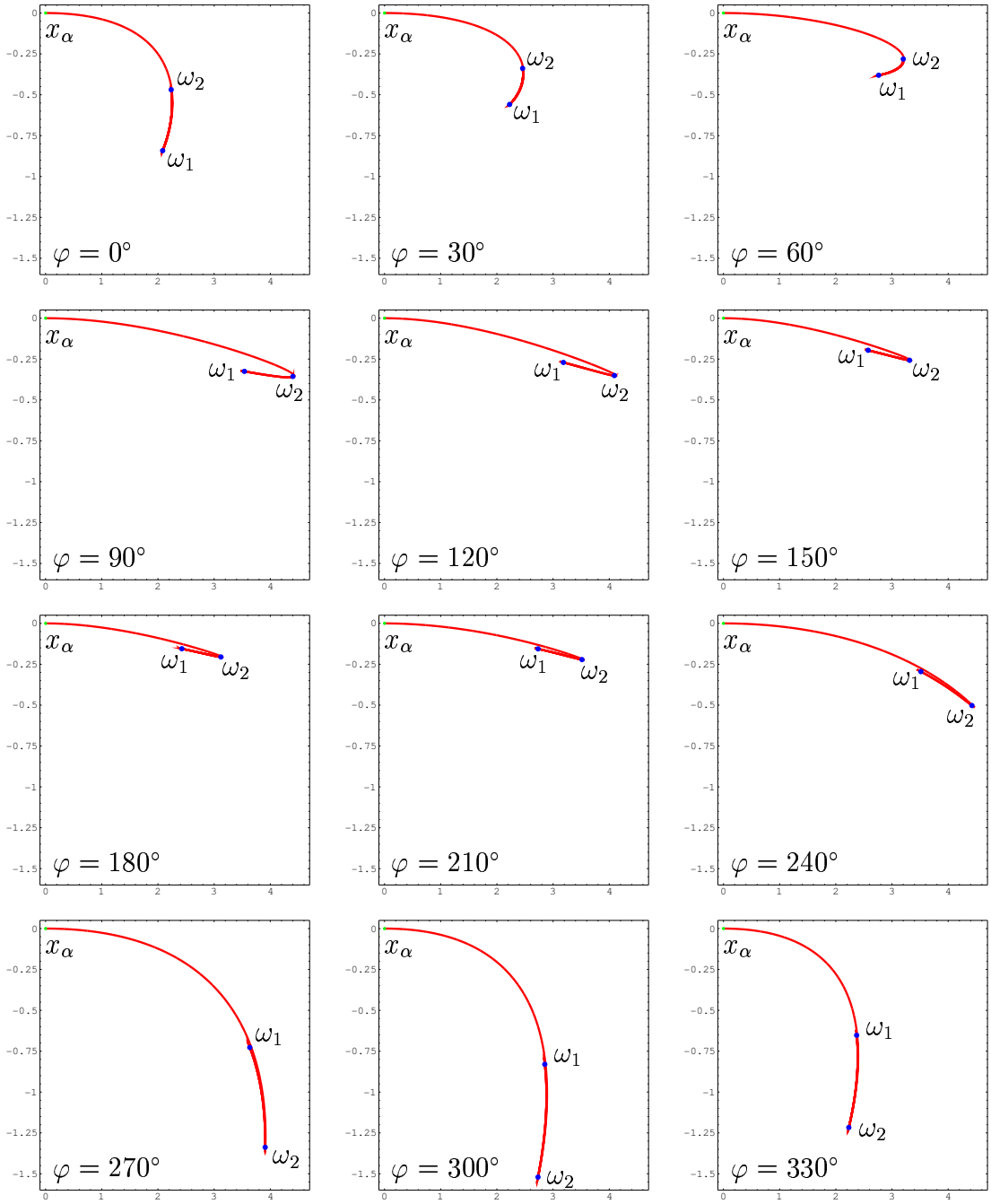

Figure 14: *The two-dimensional orientable unstable manifold (red) of the saddle point $x_\alpha = (\alpha, 0, 0)$ of the ζ^3-model (2) accumulates on a period-doubled attracting periodic orbit for $\alpha = 3.2$. This accumulation process is shown in the collection of Poincaré sections $\mathcal{S}_P(\varphi)$ obtained by rotation about the x-axis. If $\varphi = 0°$ then $\mathcal{S}_P = \{z = 0\}$. Figure 13 corresponds to $\varphi = 270°$. The axes are local and relative to the position of x_α. The unstable manifold is a curve in the Poincaré section, and the period-doubled attracting periodic orbit appears as the period-two point $\{\omega_1, \omega_2\}$ (blue). Note how after one full rotation ω_1 maps to ω_2 and vice versa; see also the multimedia supplement [Osinga, 2002] for the animated version.*

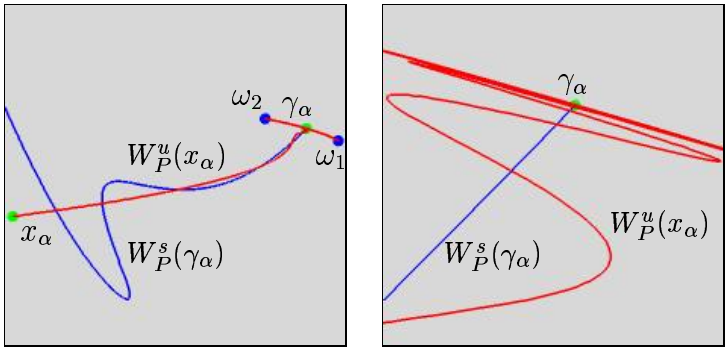

Figure 15: *The Hénon map for* $\alpha = 0.4$ *and* $\beta = 0.3$. *The one-dimensional unstable manifold* $W^u_P(x_\alpha)$ *oscillates back and forth between the period-two attractor* $\{\omega_1, \omega_2\}$ *and intersects* $W^s_P(\gamma_\alpha)$ *only on one side.*

the Poincare's section for $\varphi = 270°$; an animation of this rotation over 360° is shown in the multimedia supplement [Osinga, 2002].

The enlargements in Figs. 13(b)–(c) show that $W^u_P(x_\alpha)$ winds around the period-two points from the outside going in. The amplitude of the oscillations decreases as the manifold comes closer to the attractor and the accumulation happens on both sides. We clearly see that the manifold intersects both sides of $W^s_P(\gamma_\alpha)$. This behavior is due to the fact that, in the full state space, the stable manifold is nonorientable. Hence, as a true *first* return map, $W^s_P(\gamma_\alpha)$ shows up as two curves where P maps one curve to the other. Therefore, $W^u_P(x_\alpha)$ must intersect both sides of $W^s_P(\gamma_\alpha)$.

Surprisingly, the situation in Fig. 13 is not the "simplest" picture for planar diffeomorphisms. Intuitively, we much rather think of the following case that comes up in a typical diffeomorphism, such as the Hénon map [Hénon, 1976]:

$$(x, y) \mapsto (1 + y - \alpha x^2, \beta x). \tag{4}$$

For the "standard" parameter values $\alpha = 1.4$ and $\beta = 0.3$, chosen by Hénon, one gets the famous Hénon attractor. This attractor is created via a period-doubling sequence that can be followed in α, starting from $\alpha = 0$. For $\alpha = 0.4$ the first period-doubling just happened and we have the situation, shown in Fig. 15, where the unstable manifold of a fixed point approaches a period-two attractor. For ease of comparison, we used the same notation for the fixed points and manifolds as in Fig. 13. Comparing the two figures, we note that the accumulation in Fig. 15 happens from one side only, and the amplitude of the oscillations increases as the manifold comes closer to the attractor.

The reason that we intuitively classify Fig. 15 as the "simplest" case, is because the intersection between the stable and unstable manifolds involves only one side for both manifolds. Hence, qualitatively, this picture is "simpler" than

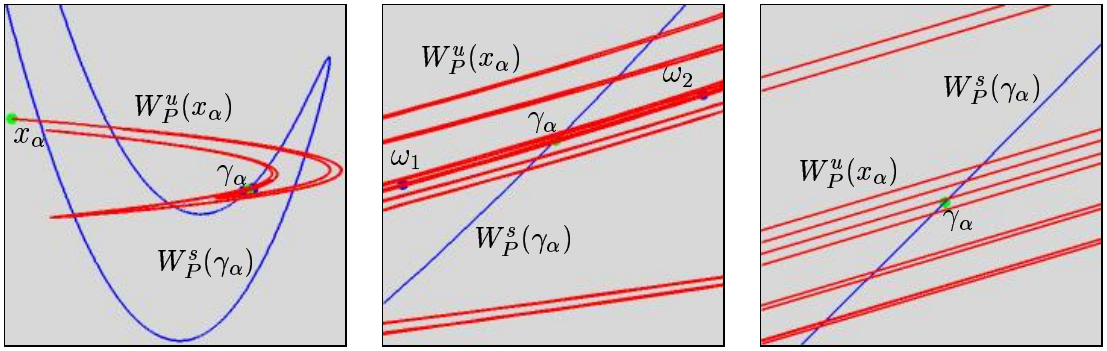

Figure 16: *The Hénon map for* $\alpha = 1.27$ *and* $\beta = -0.3$. *The situation is qualitatively the same as in Fig. 13, because the map is orientation preserving.*

Fig. 13. However, the determinant of the Jacobian of the Hénon map, which is independent of the point (x, y), is equal to $-\beta = -0.3$. That is, the map is not orientation preserving. Therefore, it cannot be the Poincaré map of a vector field in $\mathbb{R}^3$!

If we change the sign of the determinant by taking $\beta = -0.3$, we find for $\alpha = 1.27$ the situation shown in Fig. 16, which is topologically equivalent to that in Fig. 13. Even though $W^u_P(x_\alpha)$ seems to trace a much bigger attractor it really oscillates around the period-two points $\{\omega_1, \omega_2\}$ with decreasing amplitudes. As a consequence, $W^u_P(x_\alpha)$ intersects $W^s_P(\gamma_\alpha)$ on both sides, as can be seen in the enlargements.

The example of the Hénon map shows that generic phase portraits of two-dimensional diffeomorphisms can be misleading as a guide for the behaviour of three-dimensional vector fields. Furthermore, many three-dimensional vector fields with periodic orbits do not allow a globally defined Poincaré map. A study of global manifolds of Poincar'e maps that are only defined locally may lead to situations where the manifolds are no longer connected. In such situations it is crucial that the two-dimensional study be combined with a study in the full state space.

6 Nonorientable Manifolds Containing Equilibria

So far we only considered nonorientable manifolds that are stable or unstable manifolds of a twisted saddle periodic orbit Γ. For example, if we consider $W^s(\Gamma)$ then the vector field has a nonorientable invariant manifold M containing Γ and $W^s(\Gamma)$ such that M itself is repelling and the dynamics on M consists of orbits

that converge to Γ. We may think of M simply as being the closure of $W^s(\Gamma)$.

The dynamics on a nonorientable invariant manifold M may be more complicated if we allow for equilibria on M. In order to study these cases in more detail, we assume that M is a repelling manifold in the full state space and only illustrate two-dimensional phase portraits of the dynamics on M. Hence, we are dealing with the general problem of studying two-dimensional vector fields on a nonorientable manifold. However, we keep in mind that the full state space is $\mathbb{R}^3$ and that parameter variations may cause the disappearance of M.

Let us start by discussing the building blocks of M. If M is the closure of $W^s(\Gamma)$, then the building blocks are Γ and its stable manifold. If this manifold is bounded, say, by a repelling period-doubled orbit Ω, then M also contains Ω. As an illustration for more complicated dynamics on M, consider Fig. 17. Here M is depicted as a rectangle, the left and right sides of which should be identified after half a twist, as indicated by the arrows on the left and right boundaries. The left-most point on the green curve is equal to the right-most point, forming the twisted saddle periodic orbit Γ. A point on the left side of the rectangle at a particular distance *above* Γ is equal to the point on the right side of the rectangle at the same distance *below* Γ, etcetera. When embedding this picture in $\mathbb{R}^3$, we assume that the direction transverse to M is (strongly) repelling.

In Fig. 17(a) there is a saddle-source pair $\{p_1, p_2\}$ of equilibria on M. These equilibria may have appeared from the original equilibrium free situation via a saddle-node bifurcation. The building blocks of M are now Γ, its stable manifold, the equilibria p_1 and p_2, and the stable manifold of p_1 (blue). Note that the unstable manifold of p_1 (red) is already part of $W^s(\Gamma)$. In Fig. 17(a) we can still think of M as the closure of $W^s(\Gamma)$. In Fig. 17(b), where the source p_2 underwent a Hopf bifurcation creating a repelling periodic orbit, this is no longer the case. The closure of $W^s(\Gamma)$ does not contain p_2 nor its two-dimensional stable manifold, but it has a hole. However, the original nonorientable manifold M still exists and is equal to the union of the closures of $W^s(\Gamma)$ and $W^s(p_2)$. We still consider Γ and $W^s(\Gamma)$ as the key building blocks of the nonorientable manifold M, because the closure of $W^s(\Gamma)$ is indeed a nonorientable manifold, albeit with a hole in it, while the closure of $W^s(p_2)$ is orientable.

As was already mentioned in Sec. 2, rather than having a saddle-node bifurcation take place on $W^s(\Gamma)$, as in Fig. 17(a), it may take place on Γ itself. This means that on M a saddle x_1 and a node x_2 appear such that the closure of the unstable manifold of x_1 forms a smooth closed curve H that can be considered a continuation of Γ; see Fig. 18(a). The closed curve is smooth as long as the attraction towards H is stronger than attraction on H and, similarly, the expansion from H is stronger than expansion on H. Then H is called *normally hyperbolic* and has two-dimensional stable and unstable manifolds; see [Fenichel, 1971]. Since Γ was a twisted saddle periodic orbit, H is nonorientable and M is the closure of $W^s(H)$. The theory predicts that H and its (un)stable manifolds persist under small perturbations until normal hyperbolicity is lost.

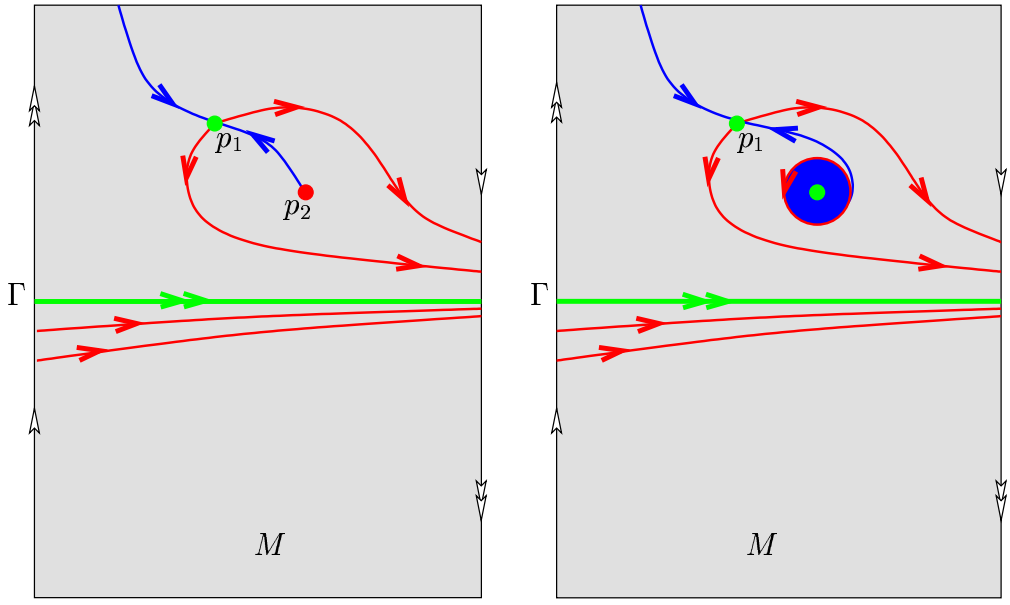

Figure 17: *Examples of dynamics on a nonorientable manifold M that contain equilibria. In this and the next figures the left and right boundaries should be glued together such that the arrows match. (a) The nonorientable manifold is formed by the closure of the stable manifold of the twisted saddle periodic orbit Γ. (b) A Hopf bifurcation can then create a hole.*

Similar to our study of bifurcations of a twisted saddle periodic orbit Γ, we now consider the loss of normal hyperbolicity of an invariant circle H as a mechanism to create or destroy nonorientable manifolds. There are several ways in which a normally hyperbolic invariant circle H can lose its normal hyperbolicity; see [Fenichel, 1971] and [Aronson *et al.*, 1982] for more details. We now describe two important cases that are well-known for orientable normally hyperbolic invariant circles; see also [Broer *et al.*, 1997].

The first possibility is that the stable eigenvalues of the attracting (on M) equilibrium x_2 become complex conjugated. This means that at x_2 the attraction towards H is of the same strength as the attraction on H. The unstable manifold of x_1 now spirals as it accumulates on x_2 and the closed curve H is no longer differentiable at x_2; see Fig. 18(b). The normally hyperbolicity of H is lost, but M still exists as the closure of $W^s(x_2)$. In the full state space $\mathbb{R}^3$ the unstable manifold of x_1 is, in fact, two-dimensional. In Fig. 18(a) this two-dimensional manifold has a smooth closure and is a nonorientable manifold that intersects M at H. Since the unstable manifold of x_1 in Fig. 18(b) spirals into x_2, the corresponding two-dimensional manifold in $\mathbb{R}^3$ has a nonsmooth closure. In other words, the unstable manifold of H in $\mathbb{R}^3$ is destroyed when H loses its normal

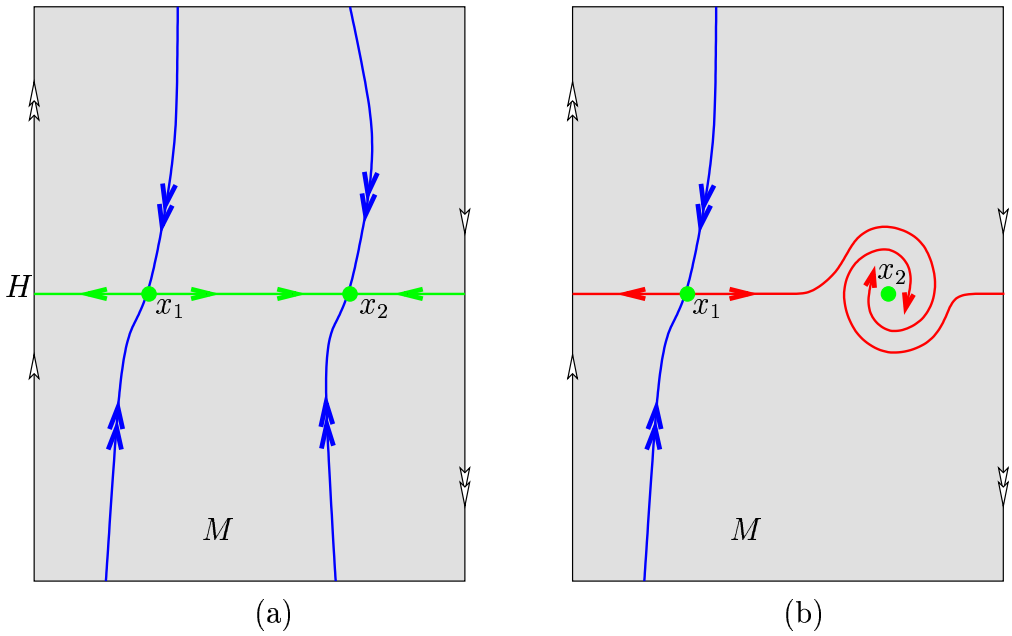

Figure 18: *Sketch of the dynamics on a nonorientable manifold M that does not contain a twisted saddle periodic orbit. (a) M is the stable manifold of a normally hyperbolic invariant circle H. (b) H lost its normal hyperbolicity due to the spiralling dynamics near x_2.*

hyperbolicity in this way.

The second possibility is that x_1 collides with an equilibrium off H. This means that x_1 and its unstable manifold disappears in a saddle-node bifurcation, which obviously destroys H. Starting from a situation as in Fig. 17(a), let us assume that a saddle-node bifurcation on M has created the saddle-source pair $\{p_1, p_2\}$. Similar to x_1, the saddle p_1 has an unstable manifold $W^u(p_1)$ consisting of two orbits that both converge to x_2. Figure 19 shows three topologically different examples of the overall arrangement of the stable, strong stable, and unstable manifolds. In Fig. 19(a) and (c) the closure of $W^u(p_1)$ (red) forms a smooth closed curve H_p which is normally hyperbolic. This normally hyperbolic circle is orientable in Fig. 19(a) and nonorientable in Fig. 19(c). Note that in both cases the nonorientable manifold M can be thought of either as the closure of $W^s(H)$ or as the closure of $W^s(H_p)$. Hence, the orientable manifold $W^s(H_p)$ in Fig. 19(a) has a nonorientable closure. We can also think of M as the closure of the orientable manifold $W^s(x_2)$.

Figure 19(a) can be transformed into Fig. 19(c) via two heteroclinic bifurcations. First, $W^u(p_1)$ forms a heteroclinic connection with the strong stable manifold of x_2. After this bifurcation, the phase portrait is as in Fig. 19(b). Both branches of $W^u(p_1)$ (red) now accumulate on x_2 from the left; the closure

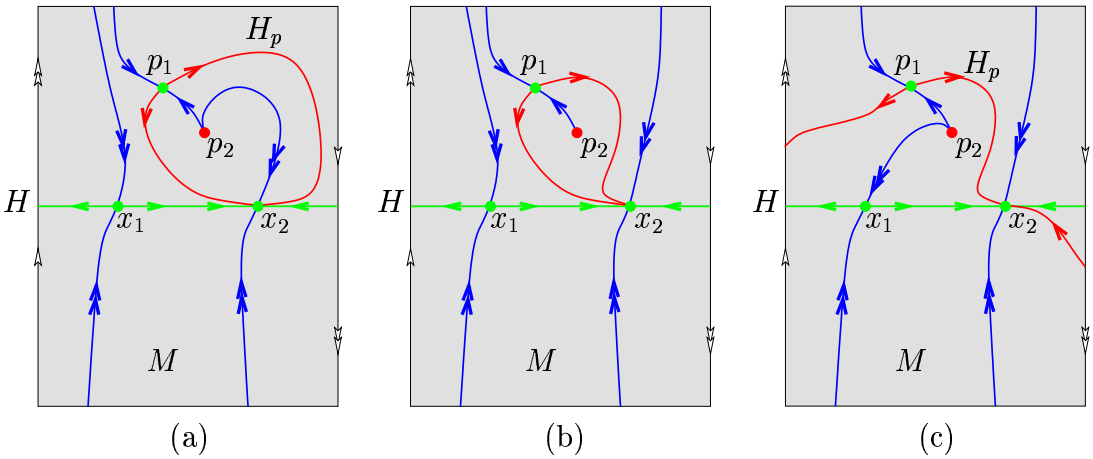

Figure 19: *Possible phase portraits on a nonorientable manifold M containing extra equilibria. In (a) and (c) a smooth normally hyperbolic invariant circle H_p is formed by the closure of the unstable manifold of p_1. This circle can either be orientable (a) or nonorientable (c). In (b) the unstable manifold of p_1 has a nonsmooth closure.*

of $W^u(p_1)$ is no longer smooth and does not form a normally hyperbolic invariant circle. Next, $W^u(p_1)$ forms a heteroclinic connection with $W^s(x_1)$. The unstable manifold $W^u(p_1)$ now makes a full turn around M (with respect to H) and on one side converges to x_2 from above and on the other side from below. The closure of $W^u(p_1)$ again forms a normally hyperbolic closed curve H_p, but now H_p is nonorientable. Other topologically different phase portraits can be obtained via additional heteroclinic bifurcations. If a normally hyperbolic circle H_p exists then it is orientable if it winds around M an even number of times (including zero times) and nonorientable otherwise.

The original question was what happens when H loses its normal hyperbolicity due to a saddle-node bifurcation of x_1 with an equilibrium off H, in our example the source p_2. This bifurcation can only take place if $W^s(x_1)$ connects to p_2, as is the case with the configuration in Fig. 19(c). When x_1 and p_2 disappear, then H is destroyed. However, the nonorientable normally hyperbolic closed curve H_p, formed by the closure of $W^u(p_1)$, remains and M persists as the closure of $W^s(H_p)$.

In the full state space $\mathbb{R}^3$, initially two nonorientable manifolds exist, namely M, as the closure of $W^s(H)$, and the closure of $W^u(H)$. The creation of the saddle-source pair $\{p_1, p_2\}$ in Fig. 19(c) leads to the appearance of $W^s(H_p)$ and $W^u(H_p)$. The closure of $W^s(H_p)$ is M, but the closure of $W^u(H_p)$ is a new nonorientable manifold. When x_1 and p_2 disappear in a saddle-node bifurcation, then there are again two nonorientable manifolds, namely M, as the closure of $W^s(H_p)$, and the closure of $W^u(H_p)$.

Finally, we remark that in Figs. 18 and 19 the nonorientable manifold M is

also the closure of $W^s(x_2)$. Hence, the two-dimensional orientable manifold of an equilibrium can have a nonorientable closure. It is not even necessary to have an equilibrium with its stable manifold in the closure of $W^s(x_2)$. The closure may be obtained by adding a single orbit (imagine the saddle is at infinity). This situation can be obtained by letting $p_1 \to \infty$, while x_1 and p_2 disappear in a saddle-node bifurcation.

7 Discussion

In this paper we discussed the creation of two-dimensional nonorientable invariant manifolds of three-dimensional vector fields. We particularly considered nonorientable stable and unstable manifolds of twisted saddle periodic orbits. Here, the manifolds are created either in a period-doubling bifurcation or in a twisted homoclinic bifurcation. We note that for the period-doubling bifurcation the nonorientability is already "built into" the system before the bifurcation in the form of two real negative stable Floquet multipliers.

We also discussed nonorientable manifolds containing equilibria. The creation of equilibria on a nonorientable manifold M happens via local bifurcations that do not influence the orientability of the manifold. If a saddle-node bifurcation takes place on the twisted saddle periodic orbit Γ, then Γ is replaced by a normally hyperbolic invariant circle H. The loss of normal hyperbolicity of H may lead to the disappearance of certain nonorientable manifolds.

Our investigations were restricted to three-dimensional vector fields. However, our observations carry over to higher-dimensional vector fields as well. For a periodic orbit of a vector field on $\mathbb{R}^n$ the product of Floquet multipliers is still positive. Hence, the negative Floquet multipliers must come in pairs. Since a nonorientable manifold is associated with an odd number of negative Floquet multipliers, we can again conclude that the stable and unstable manifolds of a saddle periodic orbit are either both orientable or both nonorientable.

In terms of the creation of nonorientable manifolds via twisted saddle periodic orbits, we use the argument that bifurcations of periodic orbits occur on center manifolds; see, for example, [Kuznetsov, 1995]. Hence, the only possible bifurcations where a single parameter is varied are the period-doubling and twisted homoclinic bifurcations, as is the case for three-dimensional vector fields. However, the possibilities for the creation of nonorientable manifolds in higher-dimensional vector fields are much richer. The nice feature of $\mathbb{R}^3$ is that any nonorientable manifold is topologically equivalent to a Möbius strip. Already in $\mathbb{R}^4$ this is no longer the case. An example is the creation of an invariant Klein bottle via a global saddle-node of limit cycles bifurcation in a four-dimensional vector field; see [Sotomayor, 1973] and [Ilyashenko & Li, 1999].

Acknowledgments

The author thanks Bernd Krauskopf for helpful discussions, in particular about Sec. 6. She also thanks Yulij Ilyashenko for pointing out that a two-dimensional nonorientable manifold may contain only one equilibrium and no periodic orbits. She is particularly grateful to the Department of Engineering Mathematics, University of Bristol, which kindly agreed to pay the copyright-fee for Fig. 1.

References

[Arneodo *et al.*, 1985] Arneodo, A., Coullet, P. H., Spiegel, E. A. & Tresser, C. [1985] "Asymptotic chaos," *Physica* **D14**, 327–347.

[Aronson *et al.*, 1982] Aronson, D. G., Chory, M. A., Hall, G. R. & McGehee, R. P. [1982] "Bifurcations from an invariant circle for two-parameter families of maps of the plane: A computer-assisted study," *Commun. Math. Phys.* **83**, 303–354.

[Broer *et al.*, 1997] Broer, H. W., Osinga, H. M. & Vegter, G. [1997] "Algorithms for computing normally hyperbolic invariant manifolds," *Z. angew. Math. Phys.* **48**(3), 480–524.

[Escher, 2000] Escher, M.C. [2000] "The graphic work," (Benedikt Taschen Verlag, Köln).

[Fenichel, 1971] Fenichel, N. [1971] "Persistence and smoothness of invariant manifolds for flows," *Ind. Univ. Math. J.* **21**, 193–225.

[Glendinning & Sparrow, 1984] Glendinning, P. & Sparrow, C. [1984] "Local and global behavior near homoclinic orbits," *J. Stat. Phys.* **35**(5-6), 645–696.

[Hénon, 1976] Hénon, M. [1976] "A two-dimensional mapping with a strange attractor," *Comm. Math. Phys.* **50**, 69–77.

[Ilyashenko & Li, 1999] Ilyashenko, Yu. S. & Li, W. [1999] *Nonlocal bifurcations* Mathematical Surveys and Monographs Vol 66 (American Mathematical Society, Providence RI).

[Johnson *et al.*, 1997] Johnson, M. E., Jolly, M. S. & Kevrekidis, I. G. [1997] "Two-dimensional invariant manifolds and global bifurcations: some approximation and visualization studies," *Num. Alg.* **14**, 125–140.

[Krauskopf & Osinga, 1998] Krauskopf, B. & Osinga, H. M. [1998] "Growing 1d and quasi 2d unstable manifolds of maps," *J. Comput. Phys.* **146**(1), 404–419.

[Krauskopf & Osinga, 1999] Krauskopf, B. & Osinga, H. M. [1999] "Two-dimensional global manifolds of vector fields," *CHAOS* **9**(3), 768–774.

[Krauskopf & Osinga, 2000] Krauskopf, B. & Osinga, H. M. [2000] "Investigating torus bifurcations in the forced Van der Pol oscillator," in *Numerical Methods for Bifurcation Problems and Large-Scale Dynamical Systems*, IMA Volumes in Mathematics and its Applications 119, eds. Doedel, E.J. & Tuckerman, L.S. (Springer-Verlag, New York), pp. 199–208.

[Kuznetsov, 1995] Kuznetsov, Yu. A. [1995] *Elements of Applied Bifurcation Theory* Applied Mathematical Sciences Vol. 112 (Springer-Verlag, New York), 2nd edition.

[Lorenz, 1963] Lorenz, E. N. [1963] "Deterministic non-periodic flow," *J. Atmos. Sci.* **20**, 130–141.

[Oldeman *et al.*, 2000] Oldeman, B. E., Krauskopf, B. & Champneys, A. R. [2000] "Death of period-doublings: locating the homoclinic-doubling cascade," *Physica* **D146**, 100–120.

[Osinga, 2000] Osinga, H. M. [2000] "Non-orientable manifolds of periodic orbits," in *Proc. of the Int. Conf. on Differential Equations, Equadiff 99 (Berlin)* Vol. 2, eds. Fiedler, B., Gröger, K. & Sprekels, J. (World Scientific, Singapore), pp. 922–924.

[Osinga, 2002] Osinga, H. M. [2002] Associated with this paper is a multimedia website that contains animations of the computed manifolds in the ζ^3-model and in Sandstede's model; the website can be found at `http://www.enm.bris.ac.uk/staff/hinke/nonorientable/`.

[Van der Pol, 1927] Van der Pol, B. [1927] "Forced oscillations in a circuit with nonlinear resistance," *London, Edinburgh and Dublin Phil. Mag.* **3**, 65–80.

[Sandstede, 1997] Sandstede, B. [1997] "Constructing dynamical systems having homoclinic bifurcation points of codimension two," *J. Dyn. Differential Equations* **9**(2), 269–288.

[Sotomayor, 1973] Sotomayor, J. [1973] "Generic bifurcations of dynamical systems," in *Dynamical systems Proc. Symp. 1971 (University of Bahia, Salvador, Brazil)*, ed. Peixoto, M. M. (Academic Press, New York), pp. 561–582.

[Spivak, 1965] Spivak, M. [1965] *Calculus on Manifolds* (Addison-Wesley, New York).

[Wieczorek *et al.*, 1999] Wieczorek, S., Krauskopf, B. & Lenstra, D. [1999] "A unifying view of bifurcations in a semiconductor lases subject to optical injection," *Optics Comm.* **172**, 279–295.

Appendix

The one-dimensional manifolds in this paper were computed with the algorithm described in [Krauskopf & Osinga, 1998]. The two-dimensional manifolds were computed with the algorithm described in [Krauskopf & Osinga, 1999] using the adaptation of [Osinga, 2000] for manifolds of twisted saddle periodic orbits. For completeness, we briefly describe how this method can be used to compute unstable manifolds of a twisted saddle periodic orbit. The stable manifold can be computed similarly by reversing time.

The main idea is the same as in [Krauskopf & Osinga, 1999]: Given a twisted saddle periodic orbit Γ, we grow the unstable manifold $W^u(\Gamma)$ starting from the linear approximation of $W^u(\Gamma)$ close to Γ. This linear approximation is the unstable normal bundle $N^u(\Gamma)$ of Γ. Locally, $N^u(\Gamma)$ can be represented by a collection of fibers $n^u(r)$ depending continuously on $r \in \Gamma$. However, since Γ is twisted, $N^u(\Gamma)$ makes half a twist, and it is impossible to choose a globally continuous set $\{n^u(r)\}_{r\in\Gamma}$.

To overcome this problem, we lift Γ to its double cover $\hat{\Gamma}$ and consider the unstable normal bundle $N^u(\hat{\Gamma})$ of the lift $\hat{\Gamma}$. Now, we can define fibered directions $\hat{n}^u(r)$ that depend continuously on $r \in \hat{\Gamma}$. More details on the particular representation that was used for the examples in this paper are given in [Osinga, 2000]. The starting data for the algorithm is a finite set of points representing a closed curve in $N^u(\hat{\Gamma})$ at a small distance δ from $\hat{\Gamma}$. To this end, we define

$$\rho_\delta = \{r + \delta\ \hat{n}^u(r) \mid r \in \hat{\Gamma}\},$$

whose projection to the original three-dimensional state space gives a closed curve that loops around Γ twice. Each side of $W^u(\hat{\Gamma})$ in the double cover space gets projected to $W^u(\Gamma)$. Therefore, we only need to compute one side of $W^u(\hat{\Gamma})$.

We can now proceed as in [Krauskopf & Osinga, 1999], as long as the computations are done in the double cover space. The adapted starting data is a finite set of points on ρ_δ. The unstable manifold is grown in concentric (topological) circles, where each new circle is computed as a set of points on the intersection of the manifold with a finite number of planes perpendicular to the last circle. Points on the new circle are a small distance Δ away from the last circle, where Δ depends on the curvature of the manifold.

More precisely, let r be a mesh point on the last circle and let $\mathcal{F}_r$ be the plane through r perpendicular to this circle. We now consider orbits that start on the last circle and intersect $\mathcal{F}_r$. Assuming that the last circle lies on the unstable manifold, these orbits are all on the unstable manifold as well. Since both $W^u(\Gamma)$ and $\mathcal{F}_r$ are two-dimensional, the intersection points of the orbits with $\mathcal{F}_r$ trace a curve locally near r. Hence, there is a unique first point on this intersection curve that lies at distance Δ from r, provided Δ is small enough. Finding this point on the new circle can be formulated as solving a boundary value problem. We refer to [Krauskopf & Osinga, 1999] for more details.